Supporting material of

Template-free synthesis of polyacrylonitrile-derived porous carbon nanoballs on graphene for efficient oxygen reduction in zinc–air batteries

Halima Begum, Mohammad Shamsuddin Ahmed, Seunghun Jung*

Department of Mechanical Engineering, Chonnam National University, 77 Yongbong-ro, Buk-gu, Gwangju 61186, Republic of Korea

Electrochemical characterization

Briefly, inks of all the as-prepared catalysts (4 mg mL^{-1} in ethanol) were prepared separately by ultrasonic agitation for 60 min to improve dispersion. The pre-polished glassy carbon electrode (GCE) was then drop coated by a 14.7 μL portion of each ink separately. The 9.8 μL of 20% Pt/C (E-TEK) suspension (2 mg mL^{-1} with 5 μL of Nafion (5%) in ethanol) was drop coated on GCE. All electrochemical techniques were recorded using a CHI 700C electrochemical workstation (U.S.A.) in high purity argon- or O_2-purged (for at least 30 min) 0.1 M KOH solution at room temperature. A carbon-rod and a saturated calomel electrode (SCE) electrode were used as counter and reference electrode, respectively. The electrode potential was determined with respect to reversible hydrogen electrode (RHE) scale according to the Nernst equation: (E_{RHE}=E_{SCE} + 0.059 pH + $E°$0.241 V, at 25 °C).

Koutecky–Levich equation

$$\frac{1}{j} = \frac{1}{j_k} + \frac{1}{j_L} \tag{1}$$

$$j_L = B\omega^{1/2} = 0.62nFA D_{O_2}^{2/3} C_{O_2} v^{-1/6} \omega^{1/2} \tag{2}$$

$$j_k = \frac{j \times j_L}{j_L - j} \tag{3}$$

where j for measured current densities (mA cm^{-2}); A for surface area of working electrode (0.196 cm^2); F for Faraday constant (96485.3 C mol^{-1}), D_{O_2} for O_2 diffusion coefficient (1.9×10^{-5} cm^2 s^{-1}); C_{O_2} for O_2 bulk concentration (1.2 mM L^{-1}); v for kinetic viscosity of 0.1 M KOH (1×10^{-2} cm^2 s^{-1}); ω for revolution speed of electrode (rpm); and B is a factor that yield from slope of j_k^{-1} vs. $\omega^{-1/2}$ plot.

Electron number and HO_2^- generation calculation:

$$n = \frac{4i_d}{i_d + (\frac{i_r}{N})} \tag{4}$$

$$H_2O_2\,\% = \frac{200\frac{i_r}{N}}{i_d + \frac{i_r}{N}} \tag{5}$$

$$N = \frac{-i_r}{i_d} \tag{6}$$

where i_d is the disk electrode current and i_r is the ring electrode current, and N is the collection efficiency of the RRDE (0.37).

Instrumental Characterization

The transmission electron microscopy (TEM) and energy dispersive X-ray spectroscopy (EDS) were carried out using a Tecnai 20 microscope at 200 kV, Crystal structure was examined by X-ray diffraction, which was carried out on a Rigaku D/max-2500, using filtered Cu Kα radiation. Detailed chemical compositions of the samples were analyzed by X-ray photoelectron spectroscopy (XPS) using a VG multilab 2000 spectrometer (Thermo VG Scientific, Southend-on-Sea, Essex, UK) in an ultrahigh vacuum using an unmonochromatized Mg Kα (1253.6 eV) radiation source and a spherical section analyzer. BET surface area and pore size distribution were obtained through the Barrett-Joyner-Halenda method by nitrogen isotherm adsorption and desorption (BelsorpII mini, BEL Japan Inc.). The Raman spectra were recorded using a LabRam HR800 (Horiba Jobin-Yvon, France) using an Ar^+ ion laser at an excitation wavelength of 514 nm.

Zn-air battery assembly

The electrochemical battery performance of the catalyst was tested using a homemade Zn–air battery, which was connected to a Land CT2001A system for data recording and collection. Briefly, the homogeneous ink was loaded on carbon fiber paper (1 cm^2) with a loading density of

0.5 mg cm^{-2} which was used as the air cathode, and a polished Zn foil was used as the anode. A 6 M KOH aqueous solution was used as the electrolyte.

DFT calculation

The structural relaxation and electronic energy calculations are computed by DFT implemented in Vienna *ab Initio* Simulation Package (VASP) [S9, S10] with Perdew-Burke-Ernzerhof functionals [S11, S12].

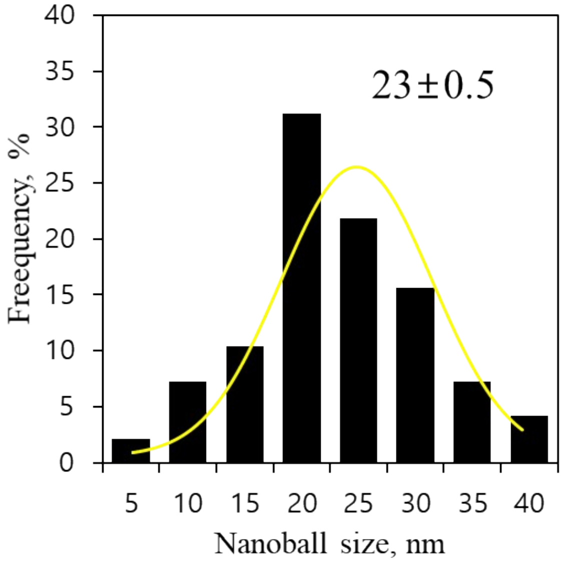

Figure S1: The size distribution of carbon nanoballs of PANRGO-700 catalyst.

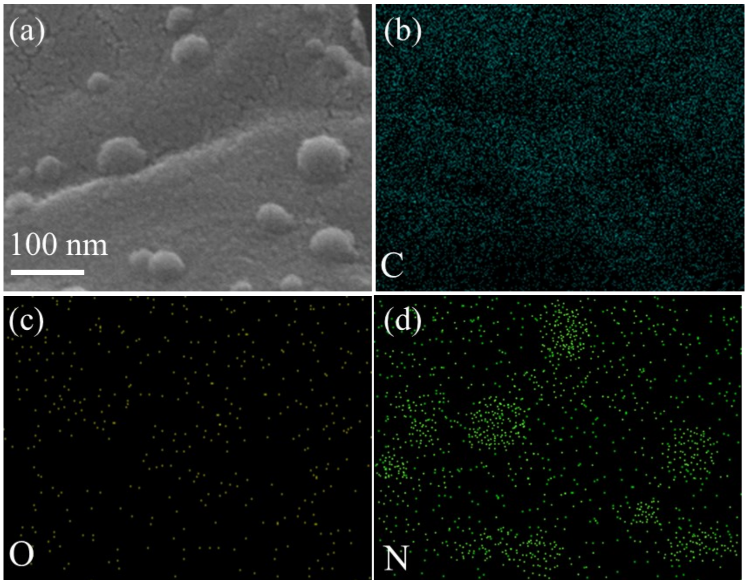

Figure S2: SEM image of PANRGO-700 (a) and the corresponding elemental mapping images of carbon (b), oxygen (c) and nitrogen (d).

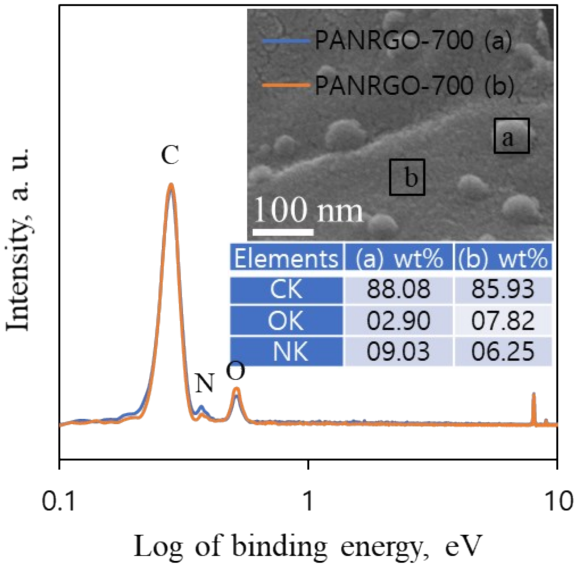

Elements	(a) wt%	(b) wt%
CK	88.08	85.93
OK	02.90	07.82
NK	09.03	06.25

Figure S3: The EDS spectra of PANRGO-700 catalyst at corresponding areas.

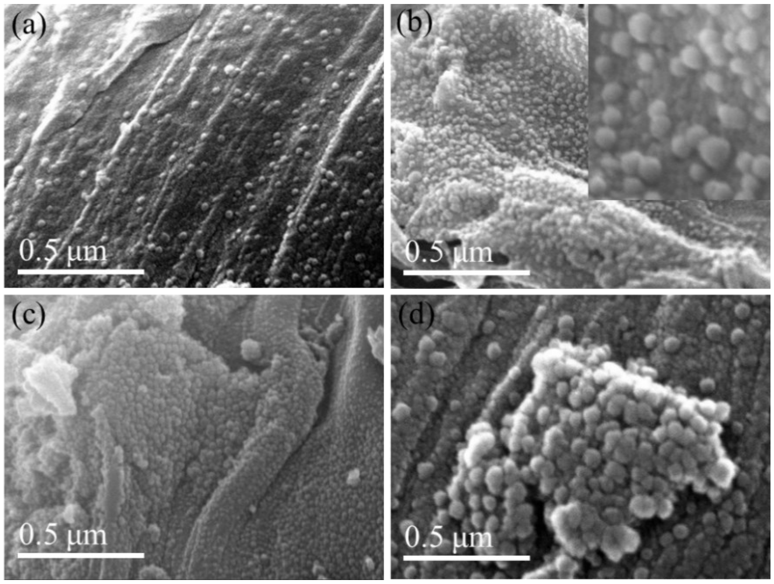

Figure S4: SEM images of PANRGO-700 with the addition ratio of GO and PAN at 1:1 (a), 1:2 (b) and 1:4 (c) with sonication for 6 hrs; and without sonication (GO and PAN ratio, 1:4) (d).

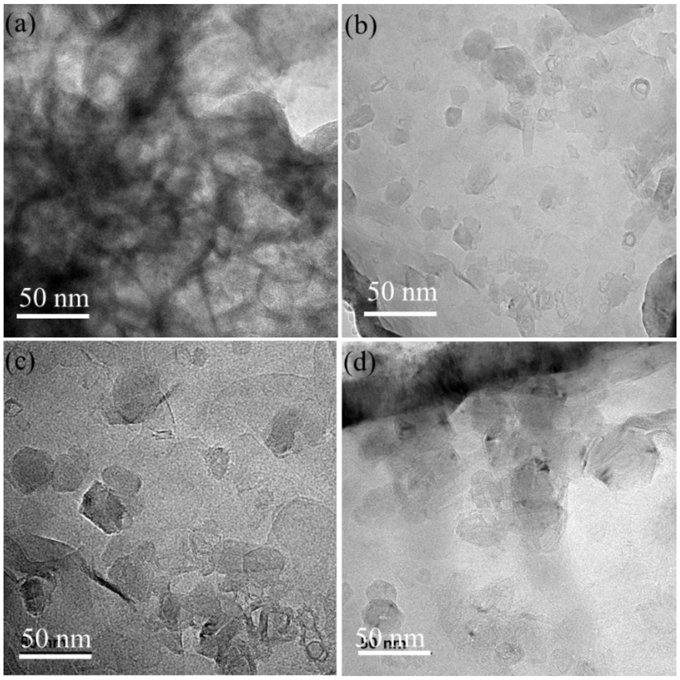

Figure S5: TEM images of PANRGO-280 (a) PANRGO-500 (b), PANRGO-600 (c) and PANRGO-800 (d) with the addition ratio of GO and PAN at 1:2 with sonication for 6 hrs.

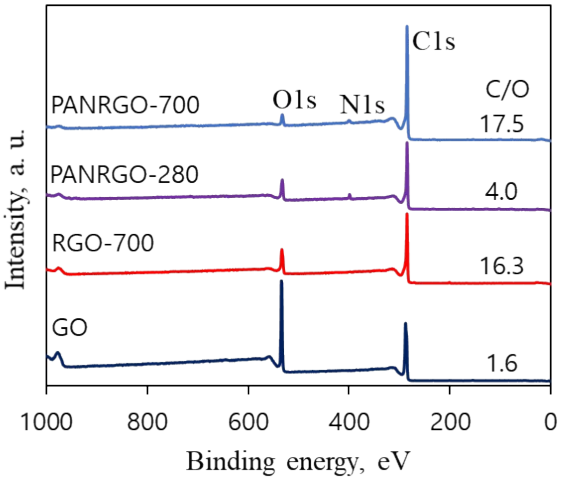

Figure S6: XPS survey spectra of GO, RGO-700, PANRGO-280 and PANRGO-700.

Table S1: The surface composition of various samples based on XPS analysis.

Sample	C 1s (at. %)	O 1s (at. %)	N 1s (at. %)
GO	61.20	38.80	
RGO-700	94.21	5.79	
PANRGO-280	70.81	17.51	11.70
PANRGO-500	78.13	10.42	11.45
PANRGO-600	83.65	6.45	9.90
PANRGO-700	85.38	4.87	9.75
PANRGO-800	89.10	5.05	5.85

Table S2: The carbon species composition of various samples based on XPS analysis.

Name	RGO-700 (%)	PANRGO-280 (%)	PANRGO-700 (%)
C=C	67.93	61.75	57.97
C–O/C–N	17.05	24.47	25.93
C=O	7.5	9.26	10.86
O–C=O	5.25	3.17	3.67
π-π* satellite	2.27	1.35	1.57

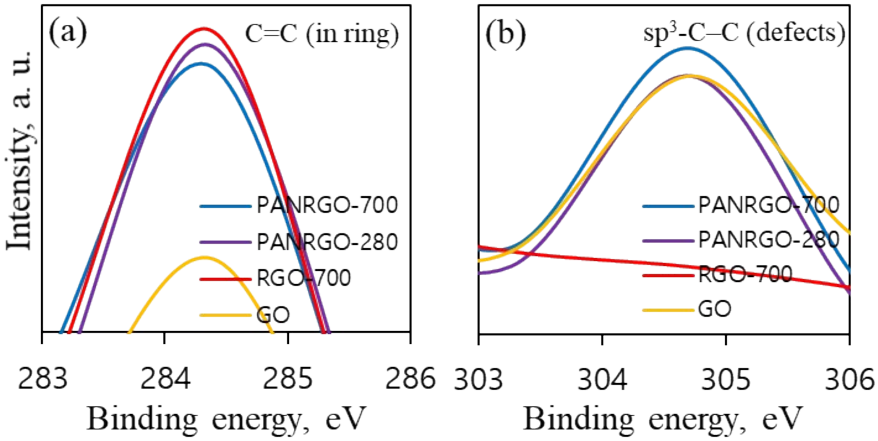

Figure S7: XANES spectra at C K-edge of GO, RGO-700, PANRGO-280 and PANRGO-700 at C=C (in ring) and sp^3-C–C (defects) peak regions.

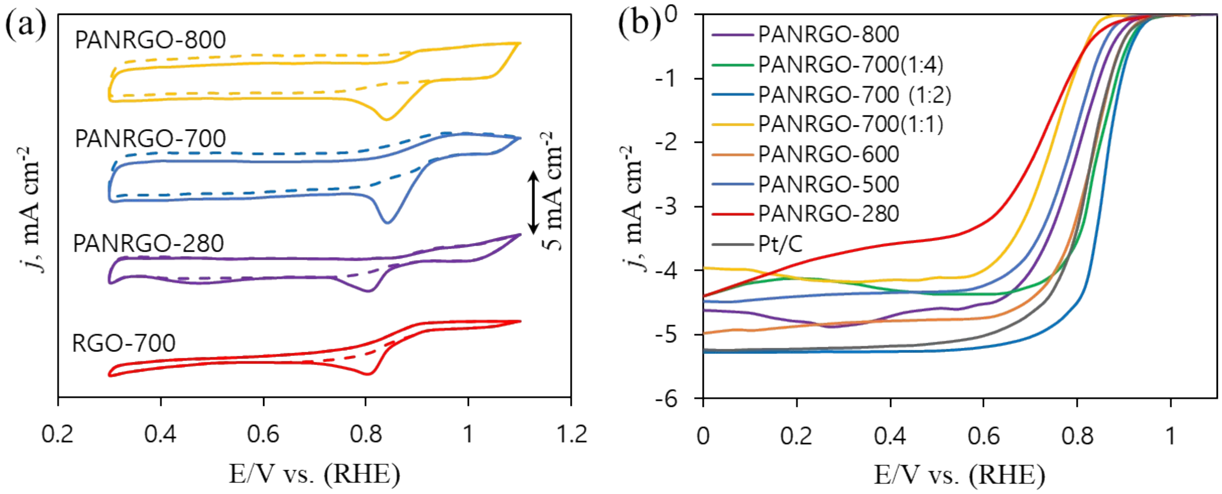

Figure S8: CV curves of different samples in Ar-saturated (dotted line) and O_2-saturated (solid line) 0.1M KOH solution at 10 mV s^{-1} (a) and LSV curves of ORR of all prepared catalysts in O_2-saturated 0.1 M KOH at a scan rate of 5 mV s^{-1} and rotation speed of 900 rpm (b).

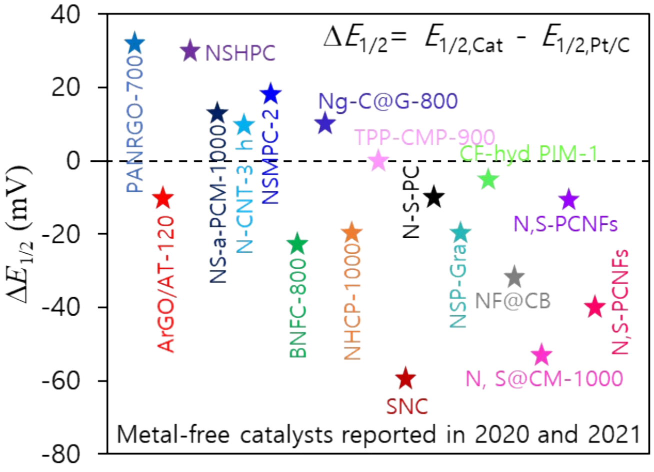

Figure S9: The comparison of ORR performance in respect to the $E_{1/2}$ of recently reported metal-free catalysts.

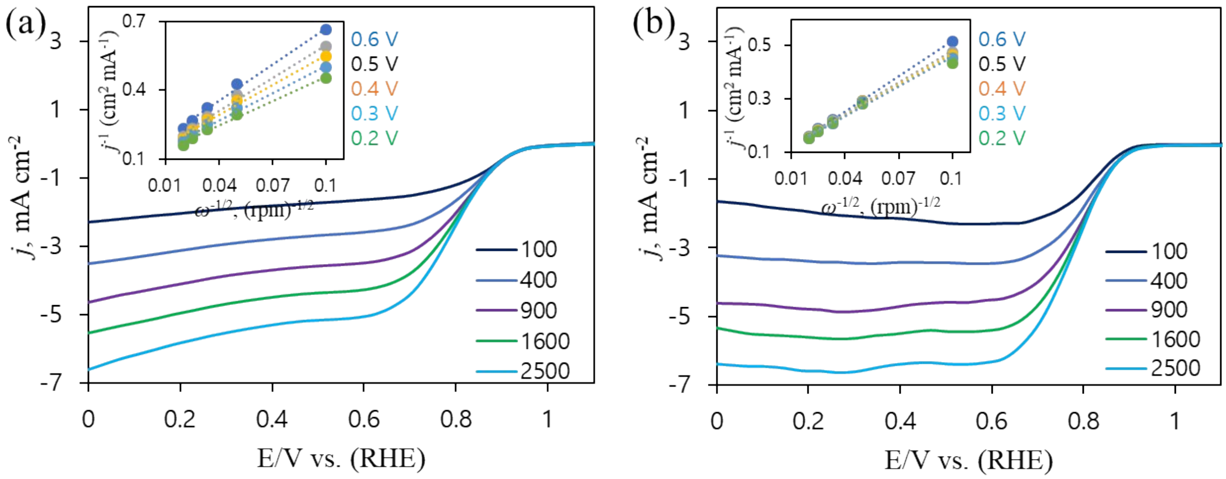

Figure S10: LSV curves of PANRGO-280 (a) and PANRGO-800 (b) in O_2-saturated 0.1M KOH solution at different rpms and at a constant scan rate of 5 mV s^{-1}, insets: the corresponding K-L plots.

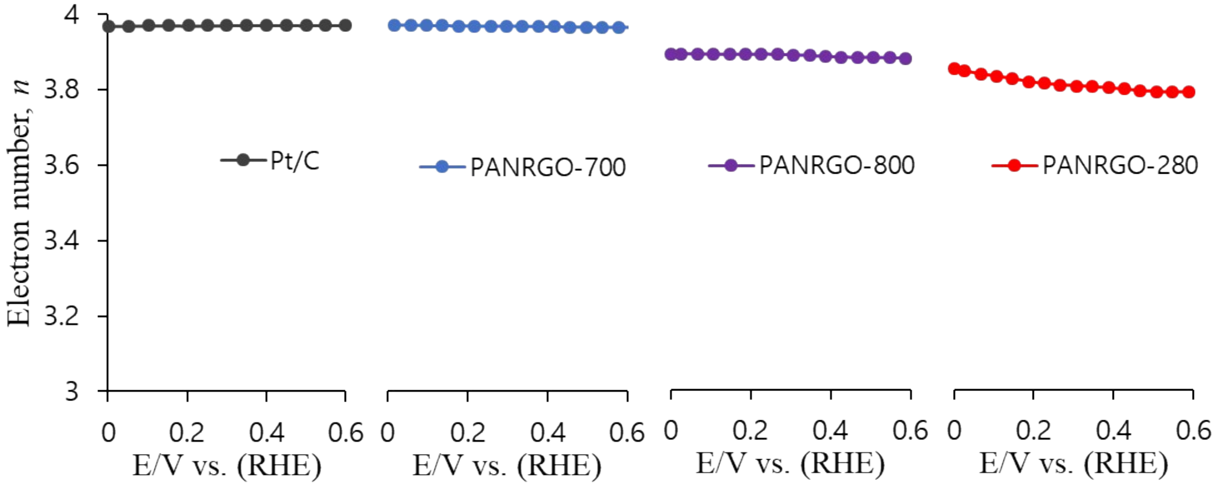

Figure S11: The calculated transferred electron numbers from K-L plots.

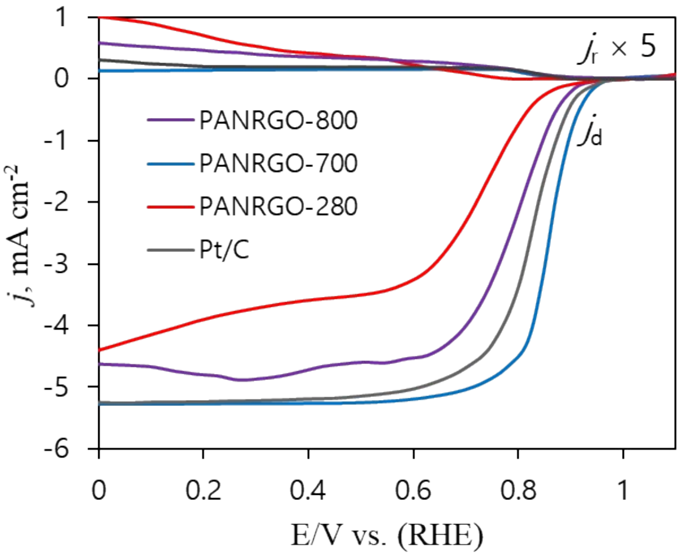

Figure S12: RRDE curves for ORR at PANRGO-280, PANRGO-700, PANRGO-800 and Pt/C in O_2-saturated 0.1 M KOH at a scan rate of 5 mV s^{-1} and rotation speed of 900 rpm.

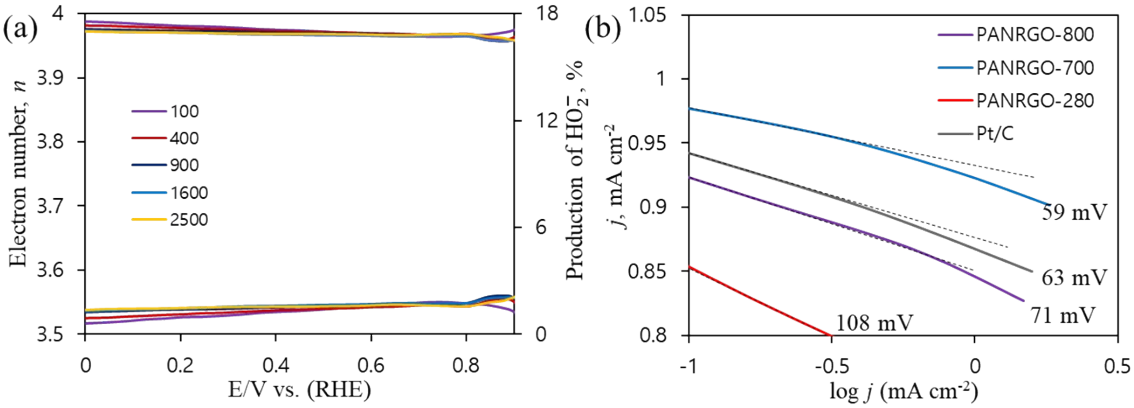

Figure S13: The n value and corresponding synthesized HO_2^- during ORR at PANRGO-700 at all tested rotation speeds (a) and the Tafel plot for ORR at PANRGO-280, PANRGO-700, PANRGO-800 and Pt/C derived from RDE curves at rotation speed of 900 rpm (b).

Table S3: The peak parameters such as peak position, FWHM and area are enlisted from XPS data.

Sample name	Elements	Peak name	Peak (BE)	FWHM (eV)	Area (N)
GO	C 1s	C=C	284.4	1.61	241.58
		C–O/C–N	285.1	1.73	102.48
		C=O	286.6	1.55	277.99
		O–C=O	288.3	1.92	85.71
RGO-700	C 1s	C=C	284.4	1.1	241.17
		C–O/C–N	285.08	1.01	34.59
		C=O	286.0	1.5	22.41
		O–C=O	288.5	2.02	16.19
		π-π* satellite	290.9	1.79	06.78
PANRGO-280	C 1s	C=C	284.4	0.92	235.41
		C–O/C–N	285.2	1.33	49.15
		C=O	285.95	2.09	32.47
		O–C=O	288.48	2.15	19.21
		π-π* satellite	290.85	3.02	05.14
	N 1s	N_1C_2	398.5	1.0	173.45
		N_1C_3	400.1	2.25	34.71
		$O_1N_1C_1$	401.85	1.3	06.22
PANRGO-700	C 1s	C=C	284.4	0.9	238.41
		C–O/C–N	285.35	1.2	58.04
		C=O	285.95	2.7	33.59
		O–C=O	288.48	1.68	17.31
		π-π* satellite	290.9	1.7	06.68
	N 1s	N_1C_2	398.5	1.9	280.65
		N_1C_3	400.8	1.65	192.02
		$O_1N_1C_1$	401.85	1.0	23.05

Table S4: The corresponding table of Figure S10.

Name	$\Delta E_{1/2}$* (mV)	Δj_L* at 0.6 V (mA cm^{-2})	*n* value at 0.6 V	References
PANRGO-700	32	0.2	3.98	This work
ArGO/AT-120	-10	0.01	3.98	6
NSHPC	30	0.3	3.92	S1
NS-a-PCM-1000	13	~0.05	3.8	S2
N-CNT-3 h	10	~0.25	>3.92	10
NSMPC-2	18	0.2	3.80	16
BNFC-800	-23	~1	3.9	S3
Ng-C@G-800	10	0.74	3.96	30
NHCP-1000	-20	0.55	~3.9	S4
TPP-CMP-900	0	-0.05	3.95	34
SNC	-60	-0.58	~3.95	66
N-S-PC	-10	-0.95	3.73	76
NSP-Gra	-20	-0.8	3.7	77
CF-hyd PIM-1	-5	-0.62	~3.9	S5
NF@CB	-32	-0.1	3.97	S6
N, S@CM-1000	-53	~0.0	~3.95	S7
N,S-PCNFs	-11	0.5	3.98	S8
N-CoS_2 YSSs	-40	-1.4	3.7	79

*$\Delta E_{1/2}$ or Δj_L = $value_{(Cat)} - value_{(Pt/C)}$

References

S1. R. Li, F. Liu, Y. Zhang, M. Guo, D. Liu, *ACS Appl. Mater. Interfaces*, 2020, **12**, 44578−44587.

S2. H. Lu, C. Yang, J. Chen, J. Li, H. Jin, J. Wang, S. Wang, *Small*, 2020, **16**, 1906584.

S3. Q. Zhang, F. Luo, Y. Ling, S. Xiao, M. Li, K. Qu, Y. Wang, J. Xu, W. Cai, Z. Yang, *J. Mater. Chem. A*, 2020, **8**, 8430–8439.

S4. J. Yan, X. Zheng, C. Wei, Z. Sun, K. Zeng, L. Shen, J. Sun, M. H. Rümmeli, R. Yang, *Carbon*, 2021, **171**, 320-328.

S5. B. Patil, B. Satilmis, T. Uyar, *J. Power Sources*, 2020, **451**, 227799.

S6. P. Zhu, J. Gao, X. Chen, S. Liu, *Int. J. Hydrogen Energy*, 2020, **45**, 9512-9521.

S7. J. Yang, F. Xiang, H. Guo, L. Wang, X. Niu, *Carbon*, 2020, **156**, 514-522.

S8. Z. He, P. Wei, N. Chen, J. Han, X. Lu, *Chem. Eur. J.*, 2020, **26**, 1–8.

S9. G. Kresse, J. Furthmuller, *Phys. Rev. B: Condens. Matter Mater. Phys.*, 1996, **54**, 11169−11186.

S10. G. Kresse, J. Furthmuller, *Comput. Mater. Sci.*, 1996, **6**, 15−50.

S11. J.P. Perdew, K. Burke, M. Ernzerhof, *Phys. Rev. Lett.*, 1996, **77**, 3865−3868.

S12. J.P. Perdew, K. Burke, M. Ernzerhof, *Phys. Rev. Lett.*, 1997, **78**, 1396−1396.